AD_____

Award Number: W81XWH-08-1-0609

TITLE: Experimental Analysis and Computational Modeling of Network States and Drug Responses in the PI3K/Akt/mTOR Network

PRINCIPAL INVESTIGATOR: John Albeck
Mentors: Walter Fontana, Gordon Mills, and Joan Brugge

CONTRACTING ORGANIZATION: Harvard Medical School
Boston, MA 02115

REPORT DATE: September 2009

TYPE OF REPORT: Annual summary

PREPARED FOR: U.S. Army Medical Research and Materiel Command
Fort Detrick, Maryland 21702-5012

REPORT DOCUMENTATION PAGE

Form Approved
OMB No. 0704-0188

1. REPORT DATE *(DD-MM-YYYY)*	**2. REPORT TYPE**	**3. DATES COVERED** *(From - To)*
01-09-2009	Annual Summary	01-Sep-2008 - 31-Aug-2009

4. TITLE AND SUBTITLE
Experimental Analysis and Computational Modeling of Network States and Drug Responses in the PI3K/Akt/mTOR Network

5a. CONTRACT NUMBER

5b. GRANT NUMBER
W81XWH-08-1-0609

5c. PROGRAM ELEMENT NUMBER

6. AUTHOR(S)
John Albeck, Walter Fontana, Gordon Mills, Joan Brugge

5d. PROJECT NUMBER

5e. TASK NUMBER

5f. WORK UNIT NUMBER

7. PERFORMING ORGANIZATION NAME(S) AND ADDRESS(ES)

Harvard Medical School
Boston MA 02115-6027

8. PERFORMING ORGANIZATION REPORT NUMBER

9. SPONSORING / MONITORING AGENCY NAME(S) AND ADDRESS(ES)

U.S. Army Medical Research and Materiel Command

Fort Detrick, Maryland 21702-5012

10. SPONSOR/MONITOR'S ACRONYM(S)

11. SPONSOR/MONITOR'S REPORT NUMBER(S)

12. DISTRIBUTION / AVAILABILITY STATEMENT
Approved for public release; distribution unlimited

13. SUPPLEMENTARY NOTES

14. ABSTRACT

Therapeutic targeting of the PI3K/Akt/mTOR pathway is expected to be highly effective against breast cancer, and numerous clinical trials are underway for compounds targeting pathway components. However, current research is revealing that the connectivity and dynamical behavior of this network is highly complex, due to numerous feedback loops and crosstalk connections. The goal of this research project is to develop quantitative models of the PI3K network that will enable the effects of inhibitors to be predicted across different types of cell lines and tumors. We have now constructed and are validating two different quantitative models of signaling in the PI3K network. The first, a mechanistic rule-based model, recapitulates the molecular steps involved in the membrane recruitment and phosphorylation of Akt. In developing this model, we have constructed a number of new experimental tools, and these have revealed a novel positive feedback loop controlling phosphorylation at Ser473, a key step in Akt activation. The second model is a data-driven model that is based on high-throughput imaging and high-content quantitation of individual cells responding to growth factors and signaling pathway inhibitors. This model seeks to link the signaling states of individual cells to the behavior of the population, and has revealed quantitative differences between normal and oncogene-driven cell proliferation in the efficiency of PI3K/Akt/mTOR signaling.

15. SUBJECT TERMS
Signal transduction, quantitative modeling, drug targeting, systems biology

16. SECURITY CLASSIFICATION OF:			**17. LIMITATION OF ABSTRACT**	**18. NUMBER OF PAGES**	**19a. NAME OF RESPONSIBLE PERSON**
a. REPORT	**b. ABSTRACT**	**c. THIS PAGE**			USAMRMC
U	U	U	UU	18	**19b. TELEPHONE NUMBER** *(include area code)*

Table of Contents

Page

Introduction

The prevalence of PI3K pathway-activating mutations in breast cancer has made this signaling network a highly attractive candidate for drug development. However, the effective use of PI3K pathway inhibitors is likely to depend critically on identifying the subsets of patients whose tumors will respond. Signal transduction pathways such as the PI3K network transmit and store information as changes in the abundance of active pathway components, such as phosphorylated kinases. Effective prediction of inhibitor efficacy will therefore require an understanding of how the signaling "state" of each cell (the integrated abundances of various pathway components) determines the cellular behaviors underlying tumor growth (proliferation and apoptosis). To establish these connections, formal quantitative models can be used to integrate experimental data on signaling states, creating a framework for predicting cellular outcomes and exploring the mechanistic relationships between pathway components [1]. Effective modeling requires a large amount of experimental data and a close relationship between model construction and experimental data collection [2]. Moreover, identifying the most effective methods of modeling signaling transduction pathways remains an important question [3].

The goal of this project is to explore two different approaches to develop formal quantitative models that link the dynamics of PI3K/Akt/mTOR pathway signaling to cell fate decisions, with the intention of predicting how signaling inhibitors will impact cellular behavior across multiple cell lines and conditions. Prototypes for each of these models have now been developed. Furthermore, the experiments performed in model construction have revealed several interesting and previously unreported aspects of PI3K/Akt/mTOR signaling. Thus, both approaches have been fruitful, and we are currently assembling two manuscripts describing our findings with each approach, which are described in detail in the sections below.

Body

Overview

Although we originally proposed to spend the first 1.5 years solely generating a large dataset (Aim 1), and the subsequent time in developing and testing models (Aims 2 and 3), we have in practice implemented a more integrated approach, in which data collection and model building are performed concurrently. This type of workflow has been shown to be a more productive approach to model construction [4], and as a result, we have already developed prototype models for each modeling approach (Aims 2 a and b) and are beginning to undertake model calibration and experimental validation (work that was originally slated for the second and third years of the grant). At the same time, dataset collection (Aim 1) is expected to continue through the coming year. Thus, the timeline of certain events has shifted, although the overall goal the experimental objectives have not changed.

Additionally, we have made a number of technical advances that have enabled the collection of data more well-suited to the planned modeling approaches. Reverse-phase protein arrays (RPPAs) were originally proposed as a data collection method for both mechanistic and data-driven modeling. However, in early experiments, it became clear that simply collecting data on total levels of phospho-Akt by RPPA would not be sufficiently informative to begin development of a detailed rule-based

mechanistic model of the pathway. We therefore developed a series of genetic constructs of various Akt isoforms that differed in mass from endogenous Akt due to the addition or deletion of domains or tags and which could therefore be resolved by electrophoresis (Fig. 1). By introducing various mutations into these constructs and by developing cell lines expressing multiple mass-resolvable isoforms of Akt, we were able to address key questions concerning the activation of Akt. Similarly, early work indicated that responses to growth factors and pharmacological inhibitors were often highly variable between cells, even within clonal populations, making population-average measurements such as those made by RPPA inadequate to address the full range of cellular states and outcomes occurring within each cell population. To address this, we developed a high-throughput immunofluorescence assay for many of the molecules in the PI3K/Akt/mTOR and related pathways, including phospho-Akt, phospho-GSK3, phospho-S6, CyclinD, phospho-Erk, Fra1, pRb, p21, p27, and p57. This technique, coupled with appropriate software, has enabled the collection of multiparameter data on thousands of single cells per well across multiple 96-well plates, thus providing a far richer data set on cellular signaling states than would be possible using population-based methods and making possible the determination of the phenotypic impact of subtle changes in signaling levels.

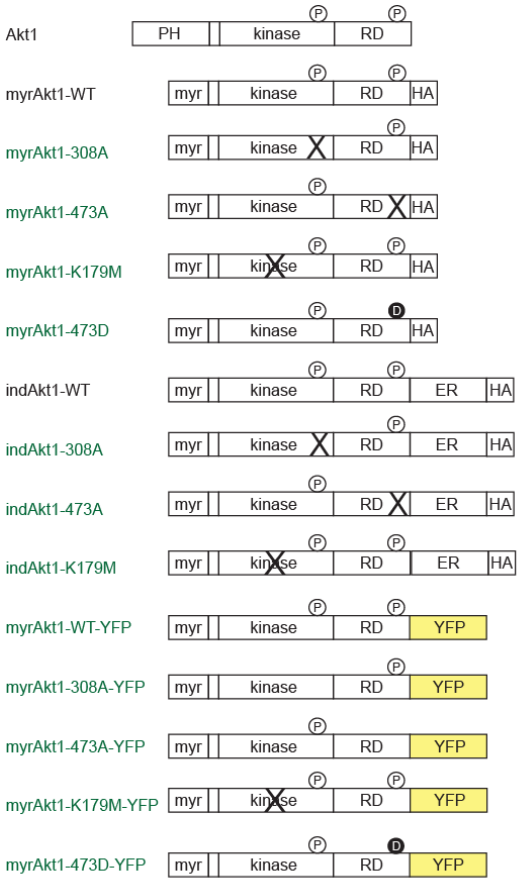

Figure 1. Akt constructs used in this study. Newly generated constructs are in green. Abbreviations: PH - plecstrin homology domain; kinase - kinase domain; RD - regulatory domain; myr - membrane-targeting myristylation sequence; HA - hemaglutinin A epitope tag; YFP - yellow fluorescent protein tag. All constructs are inserted in retroviral vector backbones.

1. Mechanistic modeling of the PI3K/Akt/mTOR pathway

As a first step in modeling the Akt pathway, we planned to use a previously described inducible version of Akt to specifically activate and measure downstream events. Since it had been reported that the phosphorylation of Akt S473 influences the substrates on which Akt is active, we generated a serine to alanine mutant at this position (S473A) [5]. As an additional control, we also generated a threonine-to-alanine mutation at the 308 position, whose phosphorylation is essential for Akt activation (T308A). As expected, induction of the non-mutant construct using 4-hydroxy-tamoxifen (4OHT) in growth factor-deprived cells led to robust phosphorylation at both T308 and S473 sites, and also led to phosphorylation of known downstream targets including GSK-3 and ribosomal protein S6 (Fig. 2). As expected, the T308A mutant failed to activate the downstream targets upon induction, but surprisingly also failed to become phosphorylated at S473, suggesting that S473 phosphorylation was dependent on Akt catalytic activity. Similarly, the S473A mutant was unable to initiate downstream signaling, and was

not phosphorylated at T308. To verify that this behavior was not an artifact of the inducible system, we produced a series of constructs that lack the inducible ER domain (Fig. 1) but retain the myristylation sequence responsible for constitutive activation. These constructs fully recapitulated the results observed with the inducible constructs. Thus, within the inducible Akt system, the phosphorylation sites T308 and S473 are highly co-dependent.

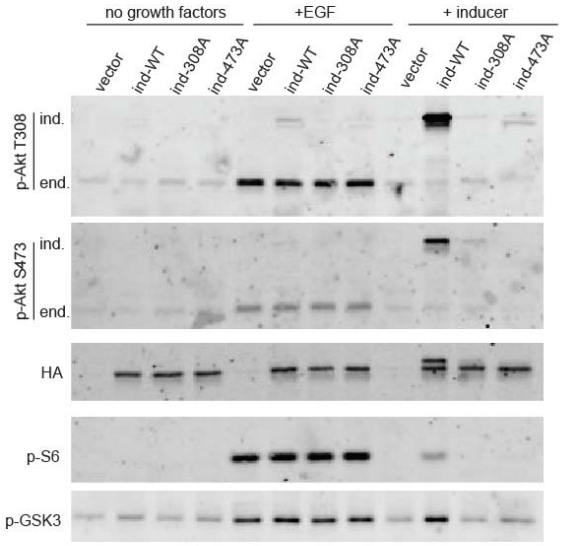

Figure 2. Co-dependence of T308 and S473 phosphorylation. MCF-10A cells expressing the indicated inducible Akt constructs were cultured in medium lacking growth factors, or supplemented with EGF or 4OHT (inducer), lysed, and subjected to immunoblot analysis with the indicated antibodies. For p-Akt T308 and S473, both the endogenous (end.) and inducible (ind.) forms were detected, at distinct molecular weights.

In parallel with these experiments, we began construction of a rule-based model of the PI3K/Akt/mTOR pathway based on all data in the current literature. However, it was quickly apparent that the observed co-dependence between S473 and T308 was not consistent with the current consensus on the mechanisms of phosphorylation at these sites – no model based on current data could reproduce such behavior. T308 is known to be phosphorylated by PDK1, and it is now believed that S473 is phosphorylated by the mTORC2 complex, suggesting that the two phosphorylation sites should be independent [5, 6]. Thus, before proceeding further with model construction, it was necessary to address this discrepancy. A broader survey of the literature revealed that similar phenomena had been observed in earlier papers, but were attributed to autophosphorylation at S473, a view that is now believed to be incorrect [7]. Indeed, in agreement with the current view, phosphorylation of myrAkt at S473 in the absence of growth factors was blocked by pharmacological inhibitors capable of disrupting mTORC1 and mTORC2 activity (including dual PI3K/mTOR inhibitors), but not by inhibitors specific for PI3K or mTORC1 alone (Fig. 3). Thus, our data, in combination with the current model, suggested a new hypothesis: Akt activity may be an upstream activator of mTORC2, leading to S473 phosphorylation and thereby stabilizing T308. Little is known about the signals upstream of mTORC2, except that it is growth factor-regulated and may be PI3K-dependent [8]. Akt is therefore a plausible candidate for an upstream signal, and this would create a positive feedback loop in which T308 and S473 are co-dependent.

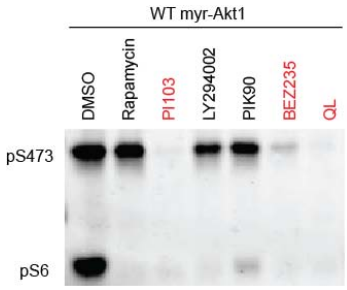

Figure 3. Requirement of mTORC2 kinase activity for myrAkt phosphorylation at S473. MCF-10A cells expressing myr-Akt1-WT were cultured in the absence of growth factors and the presence of the indicated compounds, lysed, and subjected to immunoblot analysis with the antibodies indicated at left. Compounds capable of inhibiting mTORC2 kinase activity are shown in red.

As an initial test of this hypothesis, we asked whether a phosphomimetic mutation of S473 (S473D) could restore growth factor-independent phosphorylation of T308. Indeed, myrAkt-S473D was strongly phosphorylated at T308 in the absence of growth factors and was capable of signaling to downstream targets, confirming that T308

phosphorylation requires S473 phosphorylation (Fig. 4). Furthermore, T308 phosphorylation in the non-mutant myrAkt was strongly blocked by inhibitors of mTORC2, but not by inhibitors specific for PI3K or mTORC1. Strikingly, the effects of all of these inhibitors were fully abrogated by the S473D mutation. These results indicate that mTORC2 is necessary for the sustained signaling of myrAkt in the absence of growth factors through its ability to phosphorylate S473 and thereby enable phosphorylation at T308.

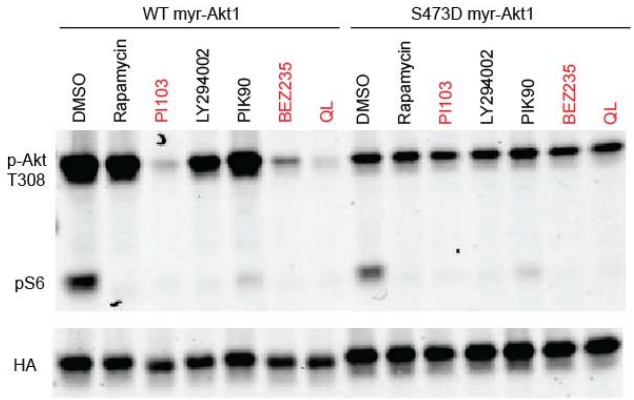

Figure 4. Loss of T308 phosphorylation upon mTORC2 inhibition and resistance of S473D phosphomimetic mutant. MCF-10A cells expressing either myr-Akt1-WT or -S473D were cultured in the absence of growth factors and the presence of the indicated compounds and subjected to immunoblot analysis with the antibodies indicated at left. Compounds capable of inhibiting mTORC2 kinase activity are shown in red.

We next examined the phosphorylation of myrAkt mutants under growth factor-treated conditions. In contrast to what was observed in the absence of growth factors, both myrAkt1-T308A and -K179M mutants were robustly phosphorylated at S473 upon addition of EGF, indicating that S473 phosphorylation does not require autophosphorylation (Fig. 5). These constructs, being permanently membrane bound, provide a useful tool for probing the activity of mTORC2 in a PI3K-indepedent manner; mTORC2 is likely predominantly localized at the plasma membrane, but endogenous Akt is recruited to the plasma membrane by PIP3 and thus will only become phosphorylated at S473 if both PI3K and mTORC2 are active. Further experiments using these constructs confirmed that the phosphorylation of S473 can be induced by insulin and IGF-1, potent activators of PI3K signaling, but is not activated by autocrine signaling induced by myristylated Akt.

We then asked whether catalytically deficient myrAkt could be phosphorylated independently of growth factors in *trans* by an exogenously expressed catalytically competent myrAkt. We therefore engineered a series of myrAkt constructs tagged at the C-terminus with YFP, enabling them to be distinguished by mass from both endogenous Akt and from untagged myrAkt. While YFP alone, or YFP-tagged myrAkt1-K179M failed to increase the level of S473-phosphorylated untagged myrAkt1-T308A in the absence of growth factors, myr-Akt1-YFP, myrAkt2-YFP, and myrAkt1-S473D-YFP all resulted in robust S473 phosphorylation of untagged myrAktT308A (Fig. 6A). In each case, this phosphorylation could be prevented by the addition of the mTOR kinase inhibitor Torin-1 [9], indicating that mTOR activity was required, and arguing against a *trans* autophosphorylation of untagged myrAktK179M by the YFP-tagged versions. Notably, we have essentially constructed a linearized version of the proposed feedback loop: myrAktS473D-YFP, which is independent of input from mTORC2 for catalytic activity, acts in an

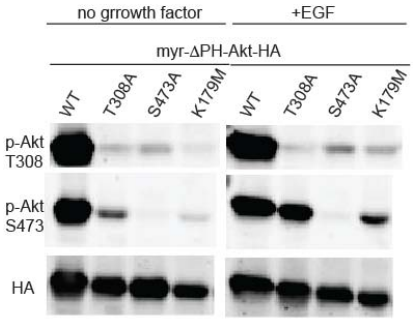

Figure 5. Response of myrAkt mutants to growth factors. MCF-10A cells expressing the indicated Akt constructs were cultured in the absence of growth factors or the presence of EGF, lysed, and subjected to immunoblot analysis with the indicated antibodies.

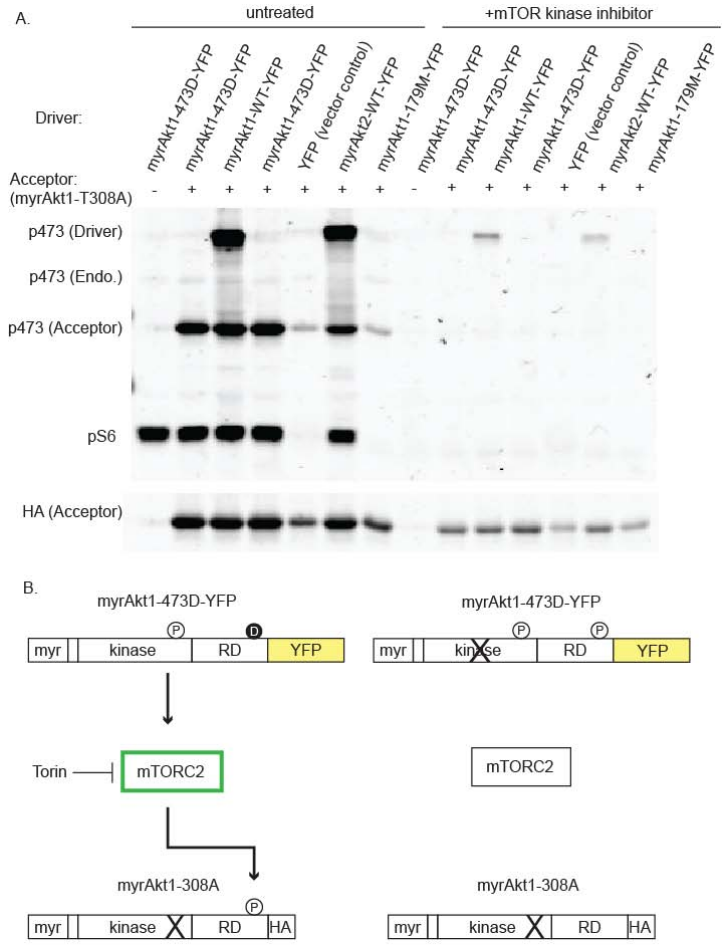

Figure 6. Linearization of the Akt-mTORC2 feedback loop. MCF10A cells were infected with viruses encoding the indicated YFP-tagged Akt1 constructs as drivers of mTORC2 activity, with or without myrAkt1-T308A as an acceptor of S473 phosphorylation. Cells were cultured in the absence of growth factors in the presence or absence of mTOR kinase inhibitor, and subjected to immunoblot anlalysis with the indicated antibodies.

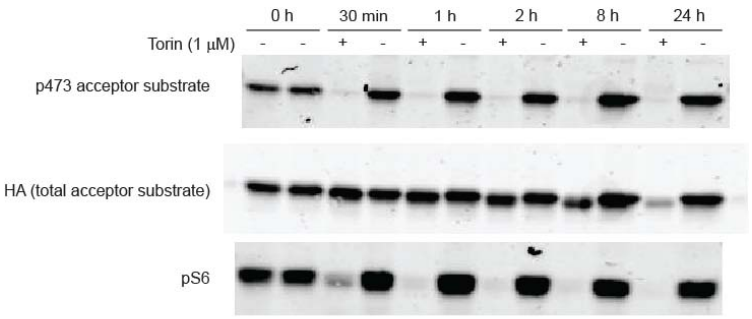

Figure 7. Kinetic separability of mTOR inhibtor effects on S473 phosphorylation and Akt protein stability. MCF-10A cells expressing myrAkt1-S473D-YFP as a driver of mTORC2 and myrAkt1-T308A as an acceptor of S473 phosphorylation were cultured in the absence of growth factors, treated with mTOR kinase inhibitor (Torin-1) for the indicated times, and subjected to immunoblot analysis.

mTOR-dependent fashion to induce the S473 phosphorylation of a catalytically inactive Akt molecule (Fig. 6B). Moreover, we note that this effect is catalytically separable from the effects of mTOR activity on Akt stability [10]: when Torin-1 is added to cells in which the linearized feedback loop is operating in the absence of growth factors, S473 phosphorylation of myrAktK179M is lost within 30 minutes, while a decrease in Akt stability, potentially due to the loss of the stabilizing mTORC2-directed phosphorylation of T450, is only observed after 8 hours (Fig. 7). Lastly, siRNA-mediated depletion of the mTORC2 component Rictor, but not of mTORC1 component Raptor, substantially reduced the ability of myrAkt-S473D-YFP to elicit phosphorylation of myrAktK179M, further confirming that this effect is mediated specifically by mTORC2 (not shown). Interestingly, depletion of TSC2, which has been reported to be important for mTORC2 activity in some contexts [8], did not have a significant effect on myrAkt-K179M phosphorylation.

As indicated in Aim 2c, our results were used to refine the core of the rule-based PI3K/Akt model. An updated core model has now been generated, and we are currently assessing its fit to experimental results using simulations.

2. Data-driven modeling of PI3K signaling

The goal of this section is to develop a model that links specific cellular signaling states to phenotypic outcomes such as proliferation or apoptosis. We

initially proposed to collect data on signaling states by RPPA and, for the same experimental conditions, data on cellular phenotypes by high-throughput microscopy or flow cytometry. In our pilot experiments, we tested a high throughput immunofluorescence (HTIF) microscopy platform, in which an automated microscope scans each well of a plate, capturing images of up to 100,000 individual cells per well in each of 4 fluorescence channels (Fig. 8). At the same time, improvements in software have made it possible to robustly analyze each image on a cell-by-cell basis, so that the signal in each cell can be individually quantitated and recorded. (The resulting data is conceptually similar to flow cytometry, but can be applied to adherent mammary epithelial cells for which flow cytometry was found to be infeasible due to the requirement for lengthy trypsinization). We found that this combination of instrumentation and software provided an extremely reliable, rapid, and robust phenotypic readout for cell proliferation when cells were stained with antibodies for phospho-pRb or Ki67. However, we also found that equally rich data on signaling states could be obtained by staining cells for proteins within the PI3K pathway, such as phospho-Akt, phospho-GSK3, and phospho-S6.

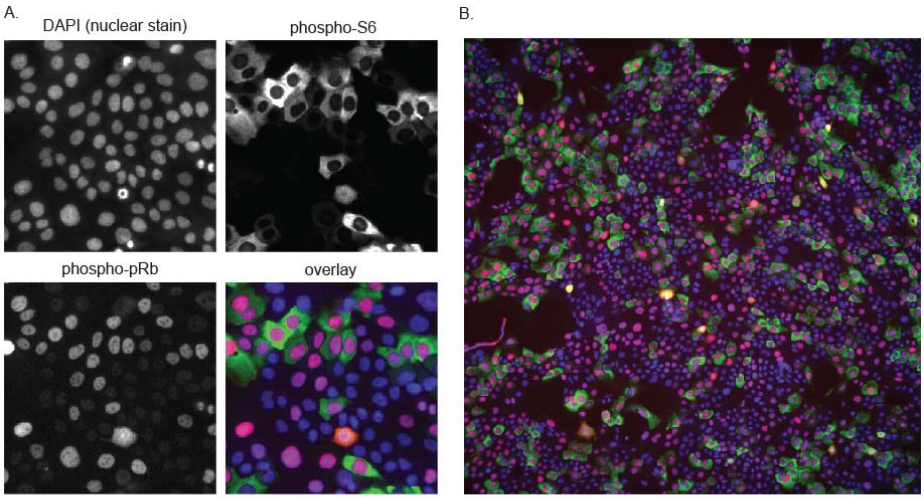

Figure 8. HTIF images of cells. MCF10A cells were cultured in the presence of 0.5 ng/ml EGF, fixed, and analyzed by HTIF for DNA (DAPI), phospho-S6, and phospho-pRb. Close-up images (A) were taken from a full field image (B) containing thousands of cells. Typically, 3-4 full field images are collected and analyzed for each well in a 96-well plate.

In analyzing the data from the HTIF platform, we noted that in many cases, both the phenotypic and signaling readouts varied substantially from cell to cell even within the same well (Fig. 8). This type of variation is not captured in formats such as RPPA, immunoblotting, or microarrays where the entire population is homogenized, resulting in a loss of information on cell-to-cell differences. Cellular heterogeneity in mammalian cell signaling is poorly understood, but recent studies have revealed it to be essential in determining cell fate decisions [11, 12]. We realized that HTIF would allow us to obtain thousands of data points for each experimental condition in which both signaling states and the resulting cell fate decision were measured for each cell. Under the originally proposed approach, each condition would produce only one population-average measurement for each signaling molecule and phenotypic readout. Thus, the HTIF platform provided a way to collect data that was much more informative and statistically rich than the original approach. These data would be more well-suited to generating a model describing the relationship between signaling and phenotype, and we therefore chose to focus on this platform as a means for generating the main dataset.

To establish the most relevant experimental conditions in which to make measurements, we performed a series of pilot experiments (Aim 1a). We initially focused on the MCF-10A cell line, which is used

extensively in the Brugge lab, and for which numerous variants expressing oncogenes are available. Treatment of these cells with a battery of inhibitors of the PI3K pathway (including LY294002, PI-103, BEZ-235, rapamycin, PIK-75, PIK-90, and Torin-1) produced potent effects on proliferation: nearly complete growth inhibition was observed at low micromolar concentrations of most inhibitors, indicating a strict requirement for the PI3K/mTOR pathway for proliferation in this cell system (Fig. 9). In contrast, no significant cell death was observed with any inhibitor (with the exception of an Akt inhibitor with relatively poor specificity, which is likely due to off-target effects), and we therefore chose to focus on proliferation as a primary phenotypic readout. We then explored the media requirements for proliferation in this system, as the growth medium for MCF-10a cells includes multiple mitogenic factors including horse serum, EGF, and insulin. While serum could be replaced with inert bovine serum albumin without a significant change in proliferation, EGF and insulin both contributed to the maximal proliferation rate obtained in growth medium. The effect of EGF was most potent; treatment with a range of EGF concentrations led to a corresponding graded increase in pRb-positive cells, from ~5% at 0 ng/ml EGF to ~90% at the full growth medium concentration of 20 ng/ml. Insulin had a weaker effect, inducing Rb phosphorylation in only ~50% of cells at saturating concentrations, but could also synergize strongly with EGF, increasing the percentage of pRb-positive cells by as much as 25% at sub-saturating EGF concentrations (Fig. 9). We therefore chose to study a set of conditions in which cells were grown in medium containing full serum and a range of different EGF concentrations, in the presence or absence of a maximal concentration of insulin, as these conditions maximized the observed variation in proliferation. Next, we examined the effects of various oncogenes, including activated (myristylated) Akt, oncogenic PI3K p110a mutants (E545K and H1047R), active HRas (G12V), and mutant or overexpressed ErbB2. Consistent with several previous reports, expression of each of these proteins (with the exception of myrAkt) enabled cells to proliferate effectively in the absence of EGF. An additional advantage of the HTIF assays was that the expression level of these proteins could be measured in each cell using an epitope tag (HA), allowing signaling and proliferation to be correlated to exogenous oncogene expression on a cell-by-cell basis. We therefore included cells expressing these proliferation-inducing oncogenes, grown in the absence or presence of EGF and insulin, as additional conditions in our dataset. Finally, we established the time points most effective for measurement. While many studies of growth factor-induced signals have concentrated on early time points where dynamic changes are largest and signals are most easily measured by immunoblot or RPPA; however, we found that following addition of growth factors or inhibitors, proliferation levels as measured by pRb or live-cell microscopy require ~20 hours to reach a new steady state that can then persist for 2-3 days until cells begin to reach confluence and are contact inhibited. Moreover, our measurements of heterogeneity in the system (see below) suggest that this steady state is actually a dynamic equilibrium, where signals fluctuate continuously at the single-cell

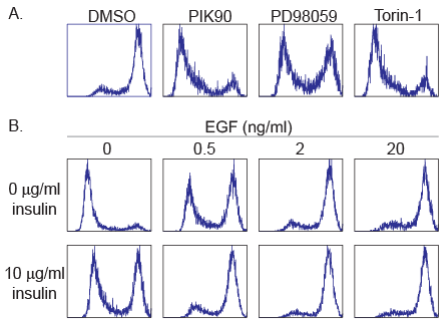

Figure 9. Effects of inhibitors and growth factors on proliferation in MCF-10A cells. A. MCF-10A cells were cultured in the presence of inhibitors targeting PI3K (PIK90), MEK (PD98059), or mTOR (Torin-1). B. MCF-10A cells were cultured in the presence of growth factors at various concentrations (B). Cells were fixed, stained for phospho-pRb, and analyzed by HTIF.

level and only appear constant when the population level is averaged as by immunoblot or RPPA. Therefore, we focused on timepoints >20 hours for optimal measurements.

The main disadvantage of the HTIF approach relative to RPPA is that fewer signals can currently be measured; while nearly 200 antibodies have been validated for the RPPA format in the Mills lab, essentially all antibodies must be re-validated for the HTIF format. Fortunately, this validation process is relatively rapid, as cellular localization, signal-to-background ratio, and growth factor/inhibitor responsiveness can be measured in a single experiment and used as stringent filters for effective antibodies (Appendix A). We applied this process to a variety of antibodies (using the RPPA-validated antibody list as a guide) and identified suitable antibodies for measuring a core set of signals involved in PI3K-induced proliferation (phospho-Akt(S473), phospho-S6, phospho-GSK3, phospho-Erk, CyclinD1/2, $p21^{Cip1}$, $p27^{Kip1}$, $p57^{Kip2}$, and Fra-1). While this initial set of signals is ~20-fold smaller than the number measurable by RPPA, it must be remembered that this lower number of signals is offset by the ~1000-fold increase in information content *per signal* afforded by the measurement of individual cells, and that a large percentage of the signals detected by RPPA are uninformative within a given context (e.g. protein signals such as total PTEN or ERK do not vary in response to growth factors or inhibitors). Both formats have similar costs (being largely antibody-dependent) and per sample turnaround times. However, HTIF is more flexible: RPPA is most efficient when hundreds of samples are accumulated over the course of weeks and run together on a single slide, while individual HTIF 96-well plates can be run daily without a loss of efficiency, allowing for rapid hypothesis testing.

To measure the relationship between signaling state and cellular outcome, we combined each signaling antibody with an antibody against phospho-pRb (hereafter pRb), which becomes phosphorylated as cells pass the restriction point and commit to proliferation, thus creating a two-parameter correlation for each signaling antibody under each experimental condition. Rb phosphorylation is essentially binary at the single cell level, allowing us to classify each cell as being either actively engaged in the cell cycle (pRb positive) or currently uncommitted (pRb negative). To examine the effect of signal strength, we binned the cellular data signal into 20 gradations along the signaling axis, and assessed the percent of pRb-positive cells within each bin (Fig. 10), and this process was repeated using both linear and logarithmic signaling scales. Thus, a curve was generated from each well, relating the strength of the measured signal to proliferative rate in the same group of cells. For signals involved in controlling proliferation a positive or negative slope should result, depending on whether the signal promotes or antagonizes proliferation, while signals unrelated to proliferation (or temporally uncoupled from their effects on proliferation) would have a slope of 0. The resulting data, discussed in

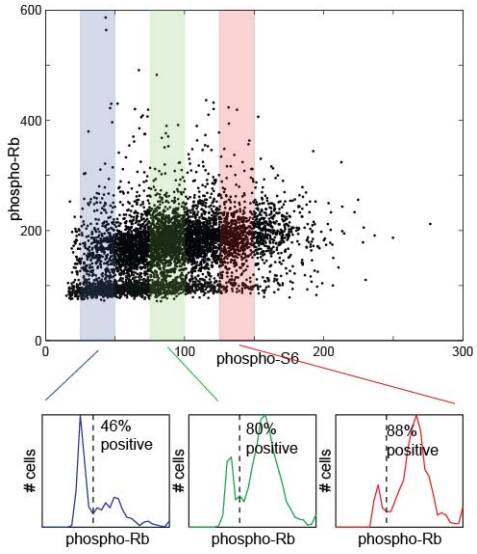

Figure 10. Analysis of proliferative state as a function of phospho-S6 levels. Raw HTIF data (scatter plot) were binned according to phospho-S6 level (colored boxes) and the fraction of phospho-pRb-positive cells was determined within each bin (histograms).

detail below, revealed an intimate association between signaling variability and cell fate, providing strong justification for continuing the single-cell approach.

One of the most notable results from these experiments was a very strong correlation between phospho-S6 levels and pRb positive cells *within* each condition (Fig. 11). Since the phospho-S6 level varied substantially from cell to cell, yet was highly predictive of the proliferative phenotype of each cell, it appears that the PI3K/mTOR pathway undergoes frequent fluctuations that are tied to cell cycle commitment. Two possibilities exist to explain this relationship: 1) the level of phospho-S6 may rise as the cell cycle progresses, resetting after mitosis, or 2) the level of PI3K/mTOR signaling may fluctuate in a way that is not determined by the cell cycle, but which determines the timing of cell cycle entry. In other words, fluctuations in signaling may be either downstream or upstream of cell cycle progression. Of these possibilities, the second appears to be most consistent with the data for several reasons. First, phospho-S6 levels show a graded response to changes in growth factor concentration, whereas purely cyclic signals such as pRb are binary and change only in the fraction of cells in the positive and negative peaks. Second, correlation of phospho-S6 signals with cell cycle position using a combination of live-cell imaging and immunofluorescence does not reveal a strong association between cell cycle timing and phospho-S6. Third, under some conditions, such as low concentrations of the MEK inhibitor P98059, cell cycle progression can be significantly altered without a corresponding change in phospho-S6 levels. Last, a role for PI3K/mTOR signaling upstream of cell cycle progression is most consistent with the well-documented role of this pathway in the control of proliferation.

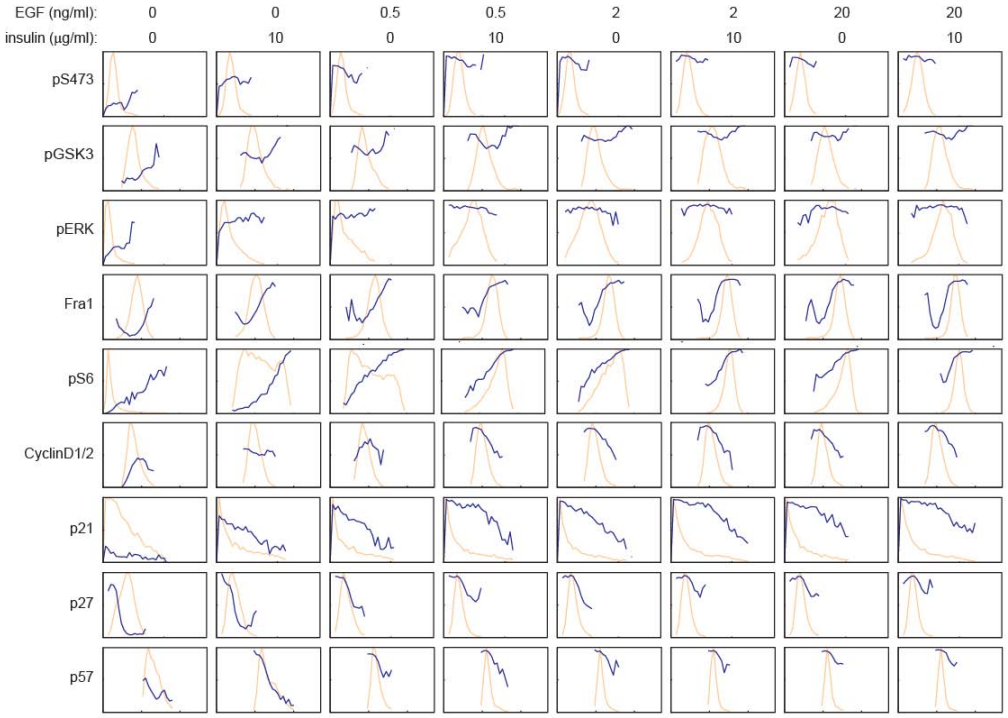

Figure 11. Analysis of proliferative state as a function of various signal levels. MCF-10A cells were cultured with the indicated concentrations of growth factors and analyzed for HTIF for phospho-Rb in combination with each of the antibodies indicated at left. The percentage of phospho-pRb positive cells as a function of signaling state (blue lines) was determined for each antibody as in Fig. 10. The intensity distributions for each signal are shown as pink lines.

We next compared the relationship between phospho-S6 and pRb across multiple conditions. Interestingly, the slope of this relationship was similar across many conditions. However, one exception to this trend was stimulation with insulin in the absence of EGF; under this condition, the phospho-S6/pRb curve was shifted to the right by a factor of ~5 relative to conditions including EGF. Similarly, when cells growing under maximal levels of EGF and insulin were treated with increasing concentrations of MEK inhibitor, the curve shifted progressively to the right. This trend also applied to cells expressing certain oncogenes, including mutant PI3K and ErbB2, and grown in the absence of growth factors also displayed a right-shifted phospho-S6/pRb curve. In these cases, the curve could be shifted back to the left by culturing the cells in the presence of EGF. Collectively, these observations can be explained by the hypothesis that proliferation is most efficient when multiple parallel pathways, including PI3K/Akt/mTor Ras/Raf/Erk, and others, are simultaneously activated. Thus, the phospho-S6/pRb curve reflects the efficiency with which PI3K/Akt/mTOR activity leads to cell proliferation. In cases where the PI3K pathway is activated but stimulation of the Ras/Raf/Erk pathway is minimal (e.g. MEK inhibition, oncogenic activation of PI3K in the absence of EGF), the level of PI3K signaling required to reach a given level of proliferation is higher relative to conditions where the ERK pathway is activated (e.g. stimulation by EGF). Intriguingly, these observations suggest that proliferation driven by oncogenes such as PIK3CA E545K may be less efficient than that stimulated by physiological lignads such as EGF. One potential implication of this situation is that the effectiveness of PI3K inhibitors may be greatest when signaling is least efficient, since lower concentrations of inhibitor would be needed to effectively eliminate the proliferative output of the PI3K pathway. Moreover, the phospho-S6/p$b curve determined by HTIF could potentially serve as an assay to identify this type of sensitivity. We plan to test these hypotheses using combinations of MEK and PI3K inhibitors on additional breast cancer cell lines.

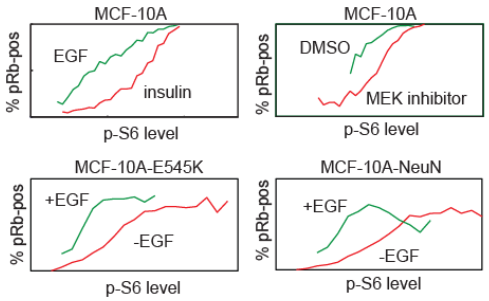

Figure 12. Proliferation induction is less efficient under conditions where the PI3K pathway is preferentially stimulated. The fraction of phospho-pRb-positive cells as a function of phospho-S6 levels were determined by HTIF and compared for the following conditions:(A) EGF vs. insulin; (B) DMSO vs. MEK inhibitor; (C) MCF-10A cells expressing PIK3CA-E545K in the presence or absence of EGF; (D) MCF-10A cells expressing NeuN in the presence or absence of EGF.

In comparison to phospho-S6, other signaling components associated with the PI3K/Akt/mTOR pathway displayed a wide range of relationships with respect to pRb. Similar to phospho-S6, Fra-1, a transcriptional target of Akt, displayed a wide dynamic range, substantial cell-to-cell variability, and a strong positive correlation with pRb. I contrast, phosphorylation of Akt at both Thr308 andSer473, displayed a relatively small dynamic range and little cell-to-cell variability across all conditions, and no significant correlation with pRb positivity was observed. Phospho-Erk and phospho-GSK3 displayed a larger dynamic range and substantial cell-to-cell variability, but like Akt did not correlate with pRb positivity. The Akt-regulated cell cycle inhibitors $p21^{Cip1}$ and $p27^{Kip1}$ both showed a strong negative correlation with pRb that was partially dependent on growth factor concentrations. Together, these results indicate that the relationship between signaling state and cellular phenotype is quite complex. A potentially critical factor determining the correlation with pRb our assay is the lifetime of active

signaling states; signals that are important but which fluctuate rapidly may show a poor correlation with phospho-Rb, because they will fail to remain positive for the signal throughout the entire time that the cell is phospho-Rb positive (~10 hours). Nonetheless, the fact that multiple proteins show a very strong correlation with pRb demonstrates that quantitative fluctuations in signaling state determine cellular behavior.

No single signal can fully determine cellular behavior, and we next examined the ability of combinations of signals to predict pRb positivity. Co-staining for the two most-predictive single signals, phospho-S6 and Fra-1 revealed that these two signals do not strongly correlate and provide independent predictive ability: pRb positivity increases with Fra-1 signal in cells where phospho-S6 is low, and vice versa (Fig. 13). When both phospho-S6 and Fra-1 are high, the effect on pRb positivity is approximately additive. Thus, phospho-S6 and Fra-1 immunofluorescence signals appear to reflect two distinct aspects of cellular signaling state.

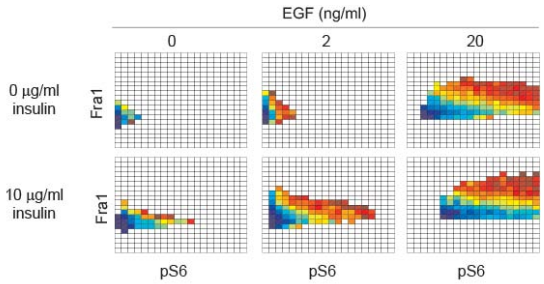

Figure 13. Analysis of proliferative state as a function of multiple signaling parameters. MCF-10A cells cultured with the indicated growth factor concentrations were subjected to HTIF analysis for Fra-1, phospho-S6, and phospho-pRb. Raw data were binned in 2 dimensions (Fra-1 and phospho-S6 intensity) to create a grid, and the fraction of phospho-pRb positive cells was determined for each grid location. Blue colors indicate a low percentage of phospho-pRb positive cells, red colors indicate a high percentage.

In constructing a model linking cellular signaling states with proliferative state, we realized that the originally proposed approach of PLSR would be inadequate, as it treats both signaling and proliferation as bulk phenomena and does not capture cell-to-cell variability. We therefore developed an agent-based approach, in which the model consists of a population of cells, or "agents", each of which has an internal signaling state and can divide to form two daughter cells that inherit characteristics of the parent. The cell cycle representation in each cell is based on the "transition probability" model of Smith and co-workers [13], in which there are two states: a B phase of fixed length that comprises S,G2,M, and the portion of G1 following the restriction point, and an A state corresponding to early G1, prior to the restriction point. The transition from A to B is a probabilistic process whose likelihood is determined by the internal signaling state of the cell. The complexity of the "signaling network" inside each cell can be set arbitrarily, and can range from a linear combination of signals as in a PLSR model to a more complex mechanistic model such as the Akt model discussed above. We are currently examining the behavior of the model using highly simplified signaling states to determine whether the model can recapitulate the observed phospho-S6, Fra-1, and p21 data. Thus far, we note that a simplified model in which a single signaling parameter fluctuates over time and controls the A -> B

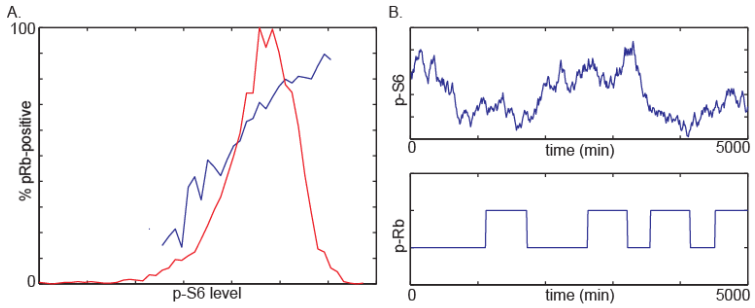

Figure 14. Computational population model of signal fluctuations and proliferative state. A MATLAB simulation of a growing population of cells, in which phospho-S6 levels fluctuate randomly and control the probabilty of cell cycle commitment. A. Simulated analysis of proliferative state as a function of phospho-S6 levels. B. Simulated time course for phospho-S6 level and phospho-Rb level for an individual cell within the population.

transition probability bears a strong resemblance to the experimental data obtained with phospho-S6 and pRb immunofluorescence. This result indicates that such a model is at least a plausible framework for the observed data and a useful starting point for continued exploration.

Key Research Accomplishments

- Generated a series of retroviral constructs and cell lines useful in tracking multiple steps in Akt activation.
- Identified a novel positive feedback loop between Akt and mTORC2.
- Constructed a basic rule-based model of Akt activation that will serve as the core for modeling the full pathway.
- Developed a high throughput single-cell assay capable of linking the status of multiple nodes in the PI3K network to cell fate decisions.
- Measured quantitative relationships between PI3K pathway nodes and cell proliferation under an array of conditions including growth factor stimulation and pharmacological inhibition.
- Generated a series of retroviral vectors and cell lines containing tagged oncogenes that can be used to measure the relationship between oncogene expression level and cell fate.
- Identified substantial signaling heterogeneity within clonal populations of mammary epithelial cells and linked this variability to changes in cell behavior.
- Constructed an agent-based population model of growth-factor stimulated proliferation.
- Optimized a high-throughput live-cell microscopy assay for cell proliferation.

Reportable Outcomes

- Manuscript in preparation detailing novel Akt-mTORC2 feedback loop.
- Manuscript in preparation describing single-cell signaling/outcome assay and the finding that signaling variability controls proliferative behavior.

Conclusion

In addition to laying the groundwork for two quantitative models of PI3K/Akt/mTOR signaling, our initial experiments have revealed a number of novel insights into the quantitative behavior of this signaling network. In developing a mechanistic model of Akt activation, our data reveal the existence of a positive feedback loop between myrAkt and mTORC2 that may be the missing link in growth factor-mediated mTORC2 activation. As we further validate this model, we are attempting to determine whether this feedback loop is required for phosphorylation of endogenous Akt. Additionally, we are extending the core model to include both upstream and downstream events and other known feedback loops. Dynamic interactions between the novel positive feedback loop and the known negative feedback loops during growth factor stimulation may help to explain some of the cell-to-cell variability observed by HTIF.

Our data showing substantial cell-to-cell variability in signaling states adds to a growing number of studies demonstrating heterogeneity in cellular responses. Importantly, our data indicate that variability in PI3K signaling is not mere “noise” or measurement error, but is functionally tied to cellular

behavior. Our data raise many questions that we are now attempting to address: What factors control cellular variability in the PI3K network? What are the timescales of the fluctuations in phosphorylation states? How does variability impact responses to pharmacological inhibitors? However, more than simply revealing new complexity, our data also suggest that cellular heterogeneity can be a powerful experimental tool, allowing subtle functional relationships to be revealed when the correct measurements are made. Thus, we plan to continue our HTIF and population modeling studies to incorporate more complex signaling networks and additional experimental conditions, including PI3K inhibitors. However, while much can be learned by continuing our HTIF studies, real-time single-cell data will ultimately be needed to determine the timescales and temporal correlations involved in signaling heterogeneity. Thus, as we continue to develop our model, we are actively exploring several techniques for collecting live-cell signaling data.

References

1. Anderson, A.R. and V. Quaranta, *Integrative mathematical oncology.* Nat Rev Cancer, 2008. **8**(3): p. 227-34.
2. Albeck, J.G., et al., *Collecting and organizing systematic sets of protein data.* Nat Rev Mol Cell Biol, 2006. **7**(11): p. 803-12.
3. Janes, K.A. and D.A. Lauffenburger, *A biological approach to computational models of proteomic networks.* Curr Opin Chem Biol, 2006. **10**(1): p. 73-80.
4. Aldridge, B.B., et al., *Physicochemical modelling of cell signalling pathways.* Nat Cell Biol, 2006. **8**(11): p. 1195-203.
5. Guertin, D.A., et al., *Ablation in mice of the mTORC components raptor, rictor, or mLST8 reveals that mTORC2 is required for signaling to Akt-FOXO and PKCalpha, but not S6K1.* Dev Cell, 2006. **11**(6): p. 859-71.
6. Sarbassov, D.D., et al., *Phosphorylation and regulation of Akt/PKB by the rictor-mTOR complex.* Science, 2005. **307**(5712): p. 1098-101.
7. Scheid, M.P., P.A. Marignani, and J.R. Woodgett, *Multiple phosphoinositide 3-kinase-dependent steps in activation of protein kinase B.* Mol Cell Biol, 2002. **22**(17): p. 6247-60.
8. Huang, J., et al., *The TSC1-TSC2 complex is required for proper activation of mTOR complex 2.* Mol Cell Biol, 2008. **28**(12): p. 4104-15.
9. Thoreen, C.C., et al., *An ATP-competitive mammalian target of rapamycin inhibitor reveals rapamycin-resistant functions of mTORC1.* J Biol Chem, 2009. **284**(12): p. 8023-32.
10. Facchinetti, V., et al., *The mammalian target of rapamycin complex 2 controls folding and stability of Akt and protein kinase C.* EMBO J, 2008. **27**(14): p. 1932-43.
11. Feinerman, O., et al., *Variability and robustness in T cell activation from regulated heterogeneity in protein levels.* Science, 2008. **321**(5892): p. 1081-4.
12. Spencer, S.L., et al., *Non-genetic origins of cell-to-cell variability in TRAIL-induced apoptosis.* Nature, 2009. **459**(7245): p. 428-32.
13. Smith, J.A. and L. Martin, *Do cells cycle?* Proc Natl Acad Sci U S A, 1973. **70**(4): p. 1263-7.

Appendix A

HTIF antibody validation experiments. MCF-10A cells were cultured under the indicated conditions and subjected to HTIF analysis with the indicated antibodies.

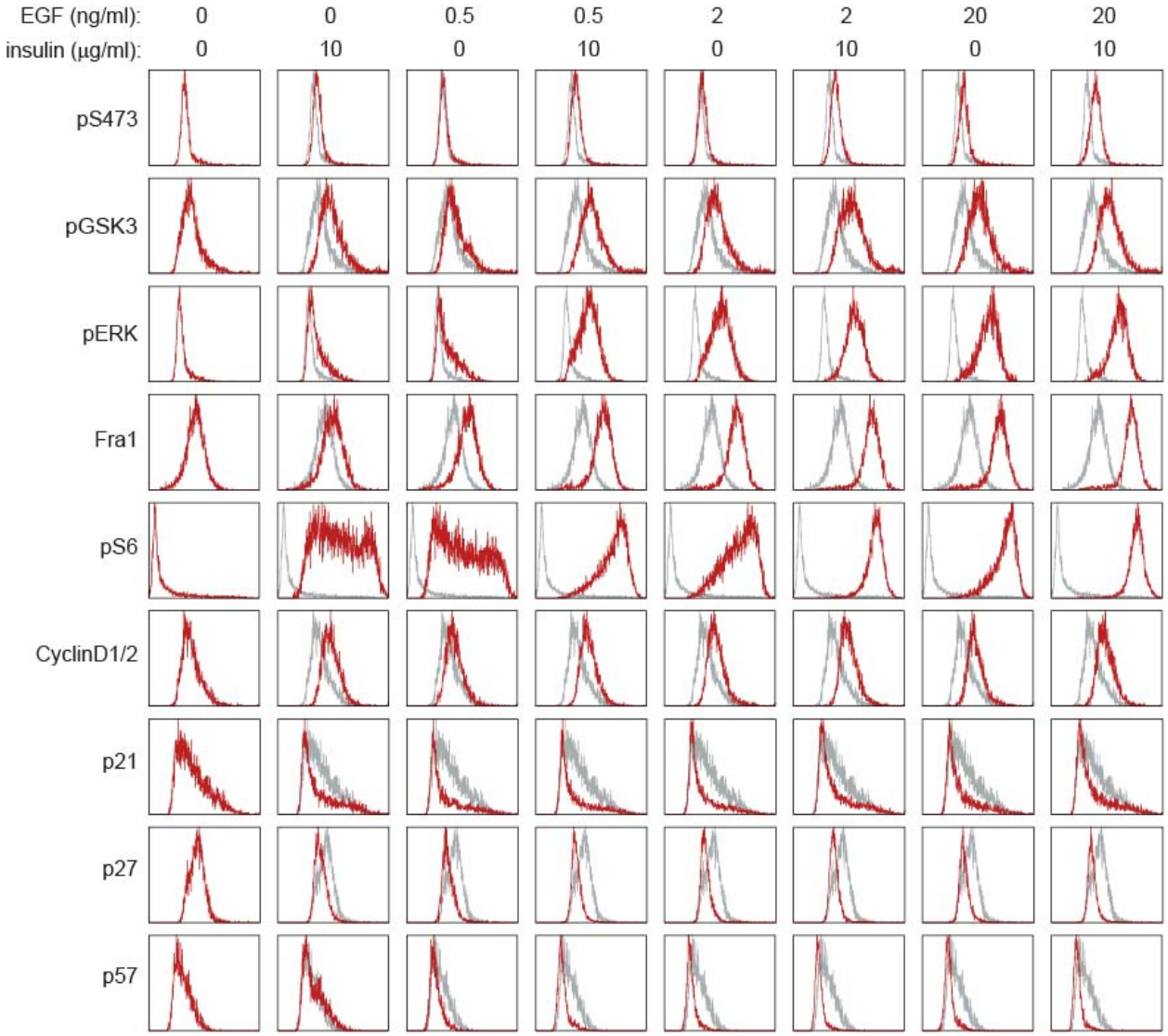

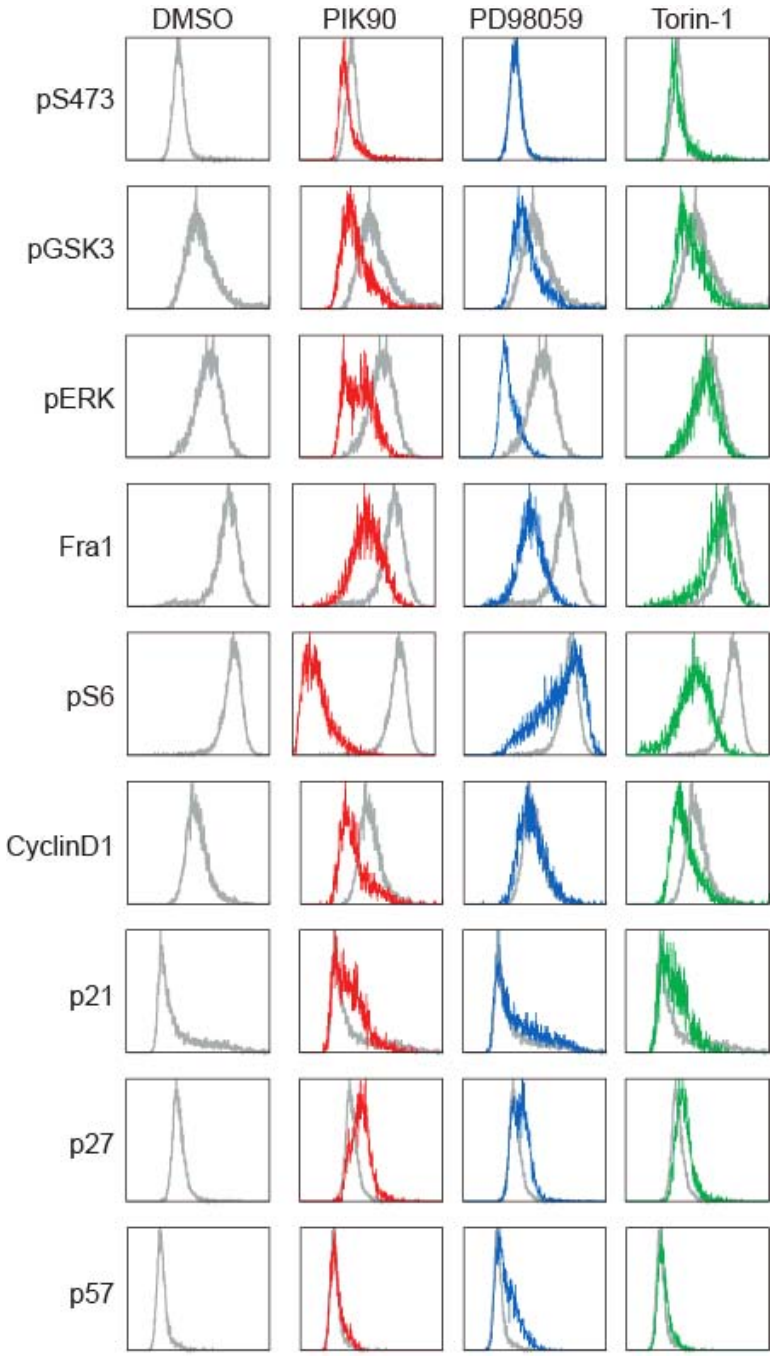
DMSO
PIK90
PD98059
Torin-1
pS473
pGSK3
pERK
Fra1
pS6
CyclinD1
p21
p27
p57